JOURNAL OF AIRCRAFT
Vol. 33, No. 1, January–February 1996

Shock Boundary-Layer Interaction on Transonic Airfoils for Laminar and Turbulent Flow

M. Swoboda* and W. Nitsche†
Technical University of Berlin, D-10587 Berlin, Germany

This article deals with the interaction between shocks and the boundary layer in a transonic airfoil flow. Here, examining comparatively the shock boundary-layer interaction in a laminar boundary layer as well as in a fully turbulent one was the main focus of interest. The experimental investigations were carried out in the transonic wind tunnel of the Technical University of Berlin. Apart from conventional time-averaging measuring techniques such as schlieren photography, Laser-2-Focus anemometry, pressure measurement, and visualization, two unsteady measuring techniques were used for investigating the dynamic effects associated with the shock boundary-layer interference. The first unsteady measuring technique concerns a new type of highly sensitive piezoreceivers and in the second technique a piezofoil array was mounted on the airfoil model. The conventional techniques already show decisive differences in the whole flowfield for the cases mentioned. At the same freestream Mach number, the position of the shock is always located further downstream for free transition. These phenomena mainly result from the development of local flow separation regions, which, on their part and with regard to their expansion and structure, strongly depend on the type of the boundary-layer flow. The unsteady measuring techniques were used to detect details in the separation regions and to determine the position of transition in the case of laminar flow. These two phenomena have a decisive influence on the global flowfield as well as on the shock boundary-layer interaction.

Nomenclature

c = profile chord
c_p = pressure coefficient
d_b = diameter of Ballotini balls
f = frequency
h = thickness of piezofoil
M = local Mach number
M_∞ = freestream Mach number
p_1 = pressure in front of shock
p_2 = pressure behind shock
p^* = critical pressure
Re = Reynolds number
x = coordinate
α = angle of attack
β = shock angle
Θ = deflection angle

Introduction

IN view of optimizing aircraft with regard to their fuel consumption, efforts have been intensified recently to develop a so-called transonic laminar airfoil (TLA) by means of which the total drag of an aircraft can be reduced up to 15%. The boundary layer of such an airfoil can be influenced by passive measures such as its design, or active ones such as boundary-layer suction in such a way that a laminar boundary layer can be maintained up to a 50–60% profile chord. As a consequence, a laminar boundary layer can possibly be maintained until the onset of shocks. In the case of the TLA developments, the interaction between a shock and the respective kind of boundary layer (i.e., laminar or turbulent) has to be taken into consideration, since the economic advantages of a subsonic laminar airfoil can be lost due to detrimental effects caused by the shock boundary-layer interference under transonic conditions.

To represent the conditions of free flight in a wind-tunnel test as realistically as possible, the transition from laminar to turbulent flow is, in most cases, fixed in the proximity of the profile nose by means of a transition strip. In the case of traditional transonic airfoils, it was quite right to assume an early transition, due to its geometry and the resulting pressure distribution. However, when compared to flight experiment, this leads to different kinds of boundary layers on the airfoil. As a consequence, the position of the transition has to be taken into consideration when applying results obtained in a wind-tunnel test to an original airfoil.

In Ref. 1 Pearcey is the first to classify in detail the different effects shocks have on the airfoil's boundary layer as well as their interaction in a fully turbulent flow. In principle, the great increase in pressure occurring due to the shock in combination with a further increase in pressure on the trailing edge causes the boundary layer to become significantly thicker. Boundary layers that are forced in such a way tend to separate. Criteria for a shock-induced local separation bubble or a complete separation are listed in Refs. 2 and 3. When increasing the Mach number or the angle of attack, the shock migrates further downstream, whereby p_1 is decreased immediately in front of the shock. In case of no separation behind the shock, p_2 increases continually behind the shock. When further increasing the Mach number, a shock-induced separation takes place, and the pressure behind the shock decreases and becomes smaller than p^*. Increasing the Mach number slightly is sufficient to cause the separation bubble to extend continually and quickly reach the trailing edge, whereby the flow separates completely and causes a decrease in the trailing-edge pressure. For this reason, $p_2 = p^*$ is postulated in Ref. 2 to be the criterion of the onset of a rapid extension of a shock-induced separation bubble.

Another criterion of a first onset of the buffeting that Pearcey lists in Ref. 4 illustrates the significance of the trailing-edge pressure for the total airfoil flow. When the separated flow reaches the trailing edge, the pressure decreases rapidly. Therefore, buffeting does not take place by definition until the trailing-edge pressure is greater than $\Delta c_{p\mathrm{TE}} = 0.05$ at a

Received Jan. 21, 1995; revision received July 24, 1995; accepted for publication July 24, 1995.

*Dr.-Ing., Research Scientist; currently at BMW Rolls Royce, Eschenweg 11, D-15827 Dahlewitz, Germany.
†Professor Dr.-Ing., Department of Aeronautics and Astronautics, Marchstr. 14.

constant lift coefficient and an increasing Mach number and angle of attack, respectively.

Buffeting is due to the unsteady behavior of shocks on airfoils. Here, local and global regions of separation oscillate due to shock fluctuation, and thus, cause the pressure distribution and, consequently, the aerodynamic force coefficients to vary continually. For this reason, buffeting can be considered an immediate consequence of the shock boundary-layer interference.

On the basis of the literature it has to be stated that, despite all the numerous papers dealing with the effects of shock boundary-layer interferences, there is a deficit with regard to the field of the interaction between transition and shock boundary-layer interaction. This is mainly due to the great importance that, in the past, was ascribed to the question of the applicability of results obtained in wind-tunnel tests, at least when considering the determination of integral coefficients. Because of rather small Reynolds numbers, this demand is controversial when dealing with smaller transonic tunnels. For this reason, the region of interference is to be examined in detail in this article for both an originally laminar and a turbulent boundary layer by means of different steady and unsteady measuring techniques.

Test Facilities

Test Section and Test Periphery

The experimental investigations were carried out at the transonic wind tunnel of the Technical University of Berlin. The tunnel is continually operated in suction mode. The experiments used a two-dimensional adaptive test section which, according to the model and adaptation, tolerates freestream Mach numbers up to $M_\infty = 0.85$ (Fig. 1). The dimensions of the test section are $150 \times 150 \times 990$ mm^3 in the nonadaptive state. In the side walls, glass windows are installed in front of and behind the position of the model in order to measure the flowfield up- and downstream of the model. The airfoil model is situated between two round window panes, which allows angles of attack to vary. The airfoil used is a supercritical CAST 7/DoA1 model (Fig. 2). Because of its high sensitivity to varied flow conditions such as varying Mach numbers and angles of attack, this model is especially suited for investigating shock boundary-layer interferences or influences of the wind tunnel. The dimensions of the model are 150×100 mm^2. Consequently, the Reynolds number is $Re = 1.4 \times 10^6$ at a design Mach number of $M_\infty = 0.76$. The model is equipped with 45 pressure taps (29 on the upper, 16 on the lower side), which are arranged along a curve close to the middle section of the model.

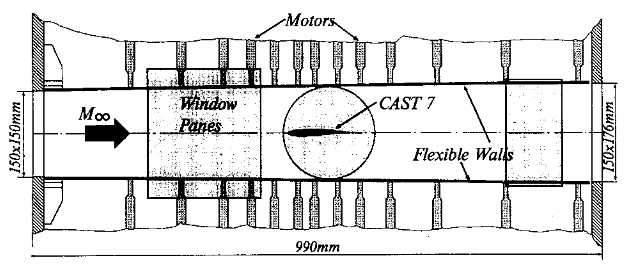

Fig. 1 Adaptive test section of the transonic wind tunnel.

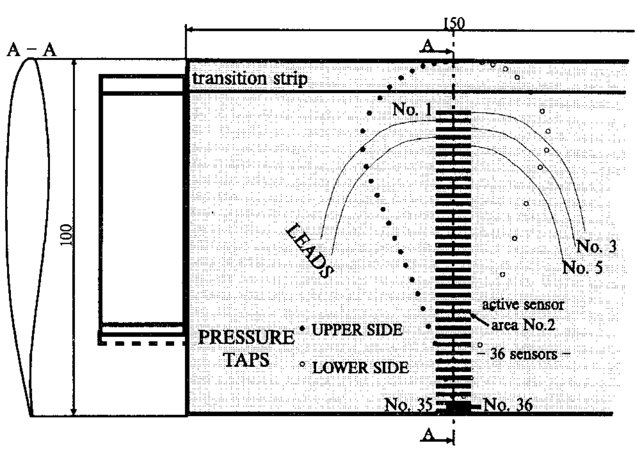

Fig. 2 CAST 7 airfoil model, position of the pressure taps and the piezofoil array.

In the investigations presented here, a new adaptation was not carried out for each variation of the Mach number, since this would have meant the introduction of a new parameter, which is difficult to evaluate with regard to shock boundary-layer interferences. For this reason, an adaptation was carried out for only two angles of attack and the design Mach number. For determining the pressure, a pounds per square inch pressure measuring system was available for simultaneously measuring up to 224 separate pressures. For measuring the flowfield globally, a Laser-2-Focus anemometer was used. Moreover, a schlieren device was employed for examining the flowfield qualitatively. In tests involving a fixed transition, a transition strip with a width of 1 mm was mounted at 7% of the depth of profile. It consisted of Ballotini balls with a diameter of $d_b = 0.1$ mm.

Piezofoil Arrays

Piezoelectric foil sensors have been successfully used in experimental aerodynamics.[6–8] Here, the basic material is an industrially produced foil made of polyvinylidene fluoride (PVDF), which was polarized by means of a strong electrical field, and thus, reacts to mechanic forces with a change of charge proportional to stress. Possible thermic tensions occurring in the foil material bring about another feature of the piezofoil, i.e., its pyroactivity or pyroelectricity.[9] Because of its small thickness ($9 < h < 100$ μm), the foil does not only react to mechanical stresses (tangential and normal forces) with a change of charge, but to the smallest change or fluctuation of temperatures.

The piezofoil works in quite a reliable way in a rather wide range of frequency of $f = 0.01$ Hz up to the region of gigaHertz (10^9 Hz). Because of its small thickness, the piezofoil is rather flexible and light and can be used quite easily. The raw foil is produced with a metal coating on both sides to be measured electrically. The material used for the coating is a rather thin layer (approximately 1 μm) made of copper, aluminium, nickel or gold. The upper and bottom coating simultaneously serve as an electrode of the foil. To partially remove the coating on one side (e.g., by etching) allows the production of regions that are sensorically active. Here, the great electric impedance of the foil material causes only regions that are coated on both sides to be sensorically active. In this way, sensor arrays can be produced that are adapted to the respective problem. Because of their flexibility and great mechanical resistance, the piezofoil can be mounted quite easily on any airfoil design with a curved surface.

Schematically, Fig. 3 shows details of the piezofoil array mounted on the upper side of an airfoil. The regions that are

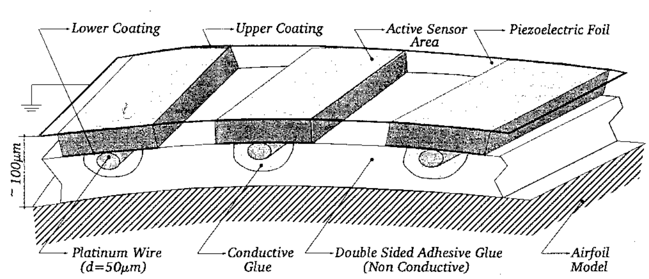

Fig. 3 Principle sketch of a piezofoil array mounted on an airfoil.

sensorically active are connected electrically to a charge amplifier by means of a platinum wire with a thickness of 50 μm. Here, the wire is linked up with the bottom coating (the hot electrode) by means of a conductive glue. The upper coating serves as a joint mass for all the sensors (the cold electrode). By means of a double-sided nonconductive glue film, in which the connecting wires are integrated as well, the foil is glued on the surface. The thickness of the foil including the glue is $\sim$100 μm.

A separate sensor worked out from a piezofoil can be produced from rather small dimensions. The dimensions typical of a sensor are between 1–20 mm^2. Thus, the sensor is, in addition, a small signal source, which is extremely sensitive to interference. For this reason, the electronics processing the signals have to be especially conceived for its respective use. Thus, the lower limiting frequency of the measuring signal to be expected is crucial for choosing the appropriate type of amplifier. Miniature receivers, which have a lower limiting frequency of f = 0.1 Hz, have proved to be most efficient in these cases.

The array used in the investigations presented here consisted of 36 separate sensors, which were arranged one behind the other in the middle section of the airfoil (Fig. 2). The distance between the separate sensors is 1.5 mm, so that the array extends from 14.5–99.5% of the depth of profile. The foil was glued along the total width of the airfoil on the upper and bottom sides in order to exclude interferences due to foil edges and three-dimensional flow effects. However, a reference pressure measurement could not be carried out in this case.

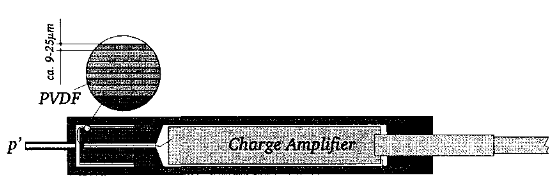

Fig. 4 Principle sketch of a piezoreceiver.

Piezofoil Receiver

Although there are reservations to be made with regard to the frequency range and the dynamics of the fluctuation quantities, linking up an external receiver with existing static pressure taps is another possibility of detecting unsteady wall shear stress on aerodynamic test bodies. Taking this problem into consideration, special piezoreceivers were developed and produced at the Technical University of Berlin (Ref. 10 and Fig. 4). In the case of this receiver, the piezofoil as well as the electronics are housed in a metal casing, where the foil is well protected against any influence of temperature and electronic interference. In this extremely small measuring volume, the foil is wound separately and several times (the area of the foil is approximately 1000 mm^2), which allows a greater specific change of charge and a greater sensitivity. The charge amplifier was designed for a lower limiting frequency of 2.8 Hz and a higher one of 5 kHz.

Because of its structure a piezoreceiver conceived in this way registers only pressure fluctuations, which means that, contrary to the case of the surface sensor, the influence of temperature and wall shear stress no longer apply here. In order not to falsify unsteady measurements to too great an extent, the connecting pressure tube was made as short as possible in order to minimize the attenuation effects and, thus, excludes possible resonance frequencies. The measurements were carried out with only one sensor since the signal characteristics of the separate sensors do not always show the same sensitivity for all of the frequencies under consideration. This excluded, however, simultaneously measuring pressure fluctuations on several pressure taps.

Results of Steady Measurements

When using conventional steady measuring techniques, great differences between a laminar and a transition-fixed flow can

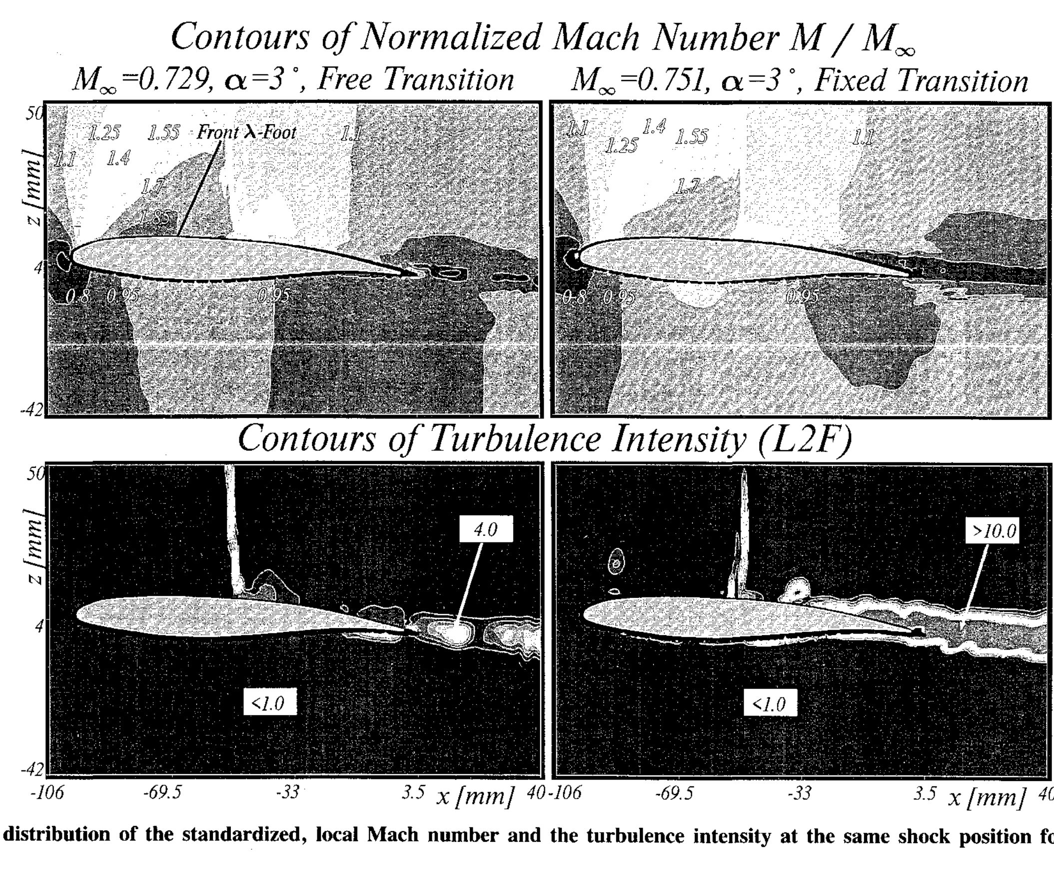

Fig. 5 L2F, distribution of the standardized, local Mach number and the turbulence intensity at the same shock position for free and fixed transition.

already be observed. In order to illustrate this fact, the global flowfield was measured by means of a Laser-2-Focus anemometry in the middle section of the airfoil. Here, the same shock position that occurs in the two kinds of flow was in the focus of interest. As a result, the freestream Mach numbers differ in the respective cases. As an example, the results of this measurement are presented in Fig. 5 at a shock position of 47% of the depth of profile. The upper parts of the figure show the distribution of the local Mach number standardized with the freestream Mach number, whereas the turbulence intensity is to be seen in the bottom parts of this figure. In both cases, the differences between free and fixed transition are to be clearly seen. In the case of free transition, the flow accelerates regularly on the upper side into the supersonic region, but slows down as early as in the middle of this region above a front foot of a λ shock, which is caused by the beginning of the separation bubble. Here, the beginning of the separation bubble has the same effect as a concave edge in the supersonic region. For this reason, the supersonic region is limited by means of a shock that is slightly curved in the upstream direction. In the case of the fixed transition, the flow is accelerated later on the upper side, and the supersonic region is limited by a vertical shock. Because of greater fluctuations, the supersonic region is also more fully developed above the airfoil in this case. Further downstream of the shock, a slight postexpansion takes place in both cases. This expansion is much more distinct in the case of free transition. In the further course of the experiment, it is to be clearly seen that the flow strongly slows down in the region of the trailing edge in the case of the fixed transition. This is due to a separation on the trailing edge. The courses of the turbulence intensity also confirm this fact. Whereas, in the case of the free transition the turbulence intensity above the airfoil and in the wake does not become greater than $Tu = 4$, it is $Tu > 10$ in these regions in the case of fixed transition. In the shock region itself, the turbulence intensity is likewise greater, because the shock is subject to lf fluctuations, whose amplitudes are often greater than the actual measuring volume of the L2F. The effect of the transition strip is clearly recognized in the courses of the turbulence intensity. It also causes the turbulence to increase considerably above the strip.

To show details of the flow in the proximity of the shock, oil visualization was carried out at the upper side of the airfoil. Here, the silicon oil used was led into the flowfield immediately behind the airfoil nose through one of the existing pressure taps in the region of high suction pressure. When compared to traditional methods of the oil film technique, this procedure has the advantage of really visualizing the actual state of the flow. In the case of free transition, a wide separation region is seen. Here, the oil spreads over the airfoil in the direction of the wingspan. The great transversal fluctuations existing in the turbulent boundary layer (fixed transition) concentrate the oil in a small separation bubble at a single place, and thus, cause distinct three-dimensional effects. In the case of free transition, the shock is to be found at the end of the separation region (determined from schlieren pictures). This illustrates that, in the case of free transition, the information on the increase in pressure is transported through the boundary layer upstream, a phenomenon that leads to flow separation. The result of the oil visualization is summarized for varied Mach numbers as well as a laminar and fully turbulent flow in Fig. 6. As a comparison, the starting position of the increase in pressure as determined from the pressure measurements is also shown in this figure.

In the case of the laminar flow, the separation bubble, which starts to develop at a Mach number of $M_\infty = 0.65$, extends up to almost 20% of the profile chord. Here, the increase in pressure above the shock always starts downstream of this separation region. This causes the separation bubble to move practically under the shock foot in the direction of the airfoil's leading edge. Starting at a freestream Mach number of $M_\infty = 0.74$, a complete separation of the flow is to be observed. It starts before the trailing-edge separation occurs. It is obvious that, in this case, the transition from the separation bubble to the complete separation takes place immediately in a rather small range of the freestream Mach number.

In principle, a separation bubble is also to be found in the case of the turbulent flow. However, its extension is much smaller, attains a maximum value of 10% of the chord at $M_\infty = 0.76$ shortly before the complete separation starts, and migrates upstream at an increasing Mach number. Here, the separation bubble and the region of complete separation al-

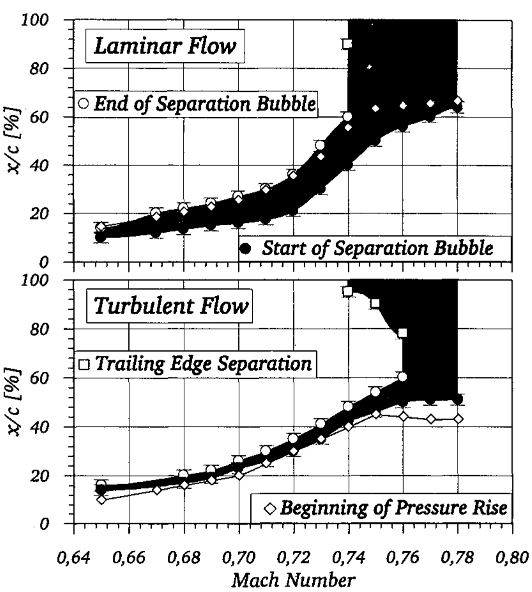

Fig. 6 Evaluation of the oil visualization, regions of separation on the airfoil for free and fixed transition, a = 3 deg.

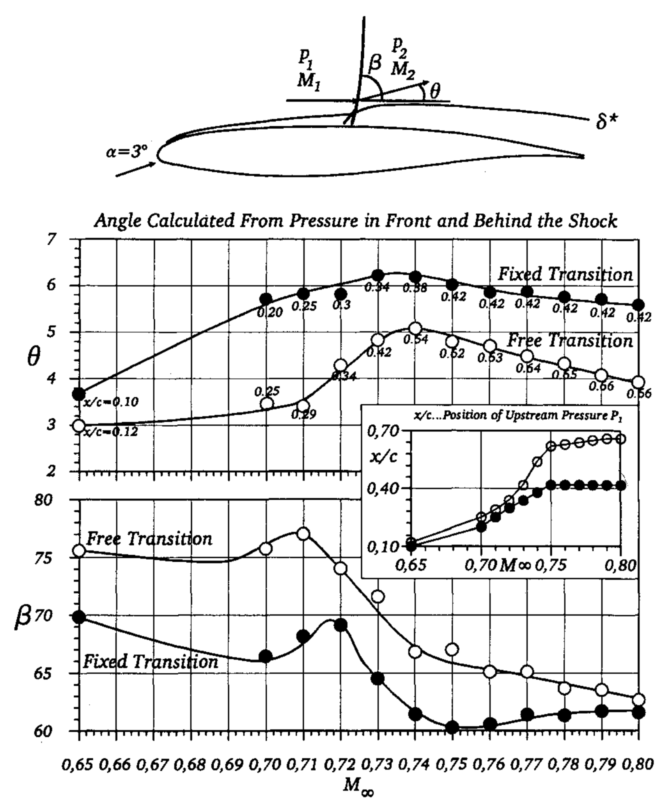

Fig. 7 Shock and deflection angle vs freestream Mach number, a = 3 deg.

ways take place behind the starting point of the increase in pressure. Although the shock intensity is greater, the increase in pressure caused by the shock cannot be transmitted upstream to the supersonic region through the fuller, turbulent boundary layer as in the case of an originally laminar flow.

Because of the different separation regions in free and fixed transition, the actual shock geometry has to differ as well in the two cases as shown in Fig. 5. To make integral statements on this problem, both the angle of shock and deflection were derived from the pressure conditions in front of and behind the shock in relation to the upper side of the airfoil by means of the shock relations. Here, we are dealing with values situated at the edge of the boundary layer, since the static pressure measured on the upper side of the airfoil is, by definition, the same as the pressure at the edge of the boundary layer. The respective results are shown in Fig. 7 in dependence on the freestream Mach number. Here, the shock angle is, at the same Mach number, always up to approximately 10 deg greater in the flow with free transition. Thus, the shock is more likely to be vertical in this case, although the shock intensity is smaller. Accordingly, the deflection angle is also smaller, which enables the streamlines to more closely follow the outline of the airfoil. This is due to a greater thickness of the turbulent boundary layer, a thickness, which on its parts, is caused by the greater increase in pressure above the shock.

Results of Unsteady Measurements

Piezofoil Array

During the first measurements carried out with the piezofoil array, time signals and power spectra were registered in the shock region to determine the different kinds of behavior that the different piezosensors show in an originally laminar and a turbulent flow. As an example, the results of these measurements are shown for an angle of attack of $a = 1$ deg and a shock position of $x/c = 46\%$ in Fig. 8. Apart from the signal courses, the power spectra of the autocorrelation and of the signal itself are presented here. For a better comparison, the autocorrelations are in addition presented linearly in a region up to 50 Hz. At first glance, the much greater signal amplitudes measured in free transition are to be recognized. Some of them are five times greater than in measurements carried out in a fixed transition flow. This fact is, of course, also reflected in the power spectra and autocorrelations. Unlike the significant and abrupt decrease of the power spectra that can be observed in the lower frequencies in the case of a fixed transition, the power spectra increase in the whole frequency region under consideration. According to expectation, the influence of the shock foot is greater in free transition. As a consequence, the shock information is transmitted along two sensors (see sensors no. 13 and 14). The power spectrum does not change significantly with regard to quality when changing above the shock. Here, a distinct frequency is not to be found. This is due to the fact that, apart from the pressure fluctuations, superposed wall shear stresses and fluctuations in temperature occur as well in the total signal of the piezofoil sensors. The larger share of the fluctuations in temperature is likely to be found in the lower frequencies. Assuming that the fluctuations in wall shear stresses are to be found in the same frequency region as the pressure fluctuations, their share in stress is to be made responsible for the rather high amplitudes in free transition, since the boundary layer has consequently to be much more unsteady due to the greater extension of the separation bubble below the shock.

Since the time signals can be registered simultaneously in the piezofoil-array measurement, new possibilities of analyzing the signals are opened up. The phase shift of the signal, e.g., can be derived in relation to the frequency from the cross correlation that takes place between two series of signals and is used for calculating the frequency response. The phase position allows then to determine the significant flow regions. When two sensors are installed in the region of a flow that is not subject to interference, their signals occur in the same phase, excluding the minimal time shift between the two sensors. When the point of separation or reattachment lies be-

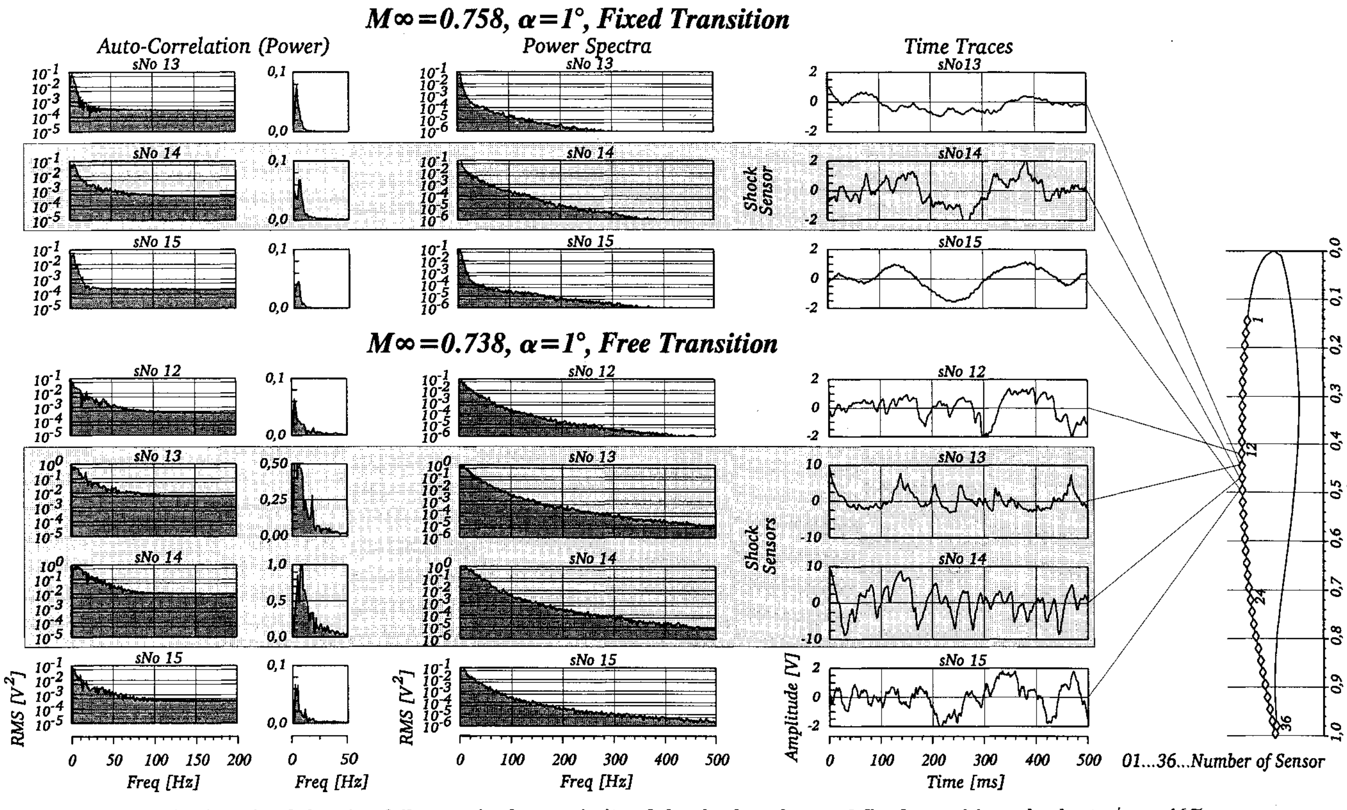

Fig. 8 Signals of the piezofoil array in the proximity of the shock at free and fixed transition, shock at $x/c = 46\%$.

tween two sensors, their signals have to be in opposite phases, since the direction of the flow and, thus, of the velocity gradient and the wall shear stress vector, respectively, change in an unsteady way. Consequently, both the fluctuations in pressure and shear stresses have to be inversely proportional at these sensors. Here, the phase shift has to be ±180 deg. At the same signal intensity, the orientation of the orbits in the Lisajous diagram is −45 deg. In Ref. 11 this principle was successfully used for detecting separation regions in the subsonic regions, whereas in Ref. 12 the exact stagnation location of an airfoil was determined in this way. Figure 9 shows the time signals, the phase shift, as well as the Lisajous diagram at a Mach number of $M_\infty = 0.724$ and $a = 3$ deg in free transition. The phase shift of 180 deg is already seen by means of the lf shares in the time signal between sensors no. 13 and 14. With the two sensors, the frequency response and the orientation of the orbits show the behavior that was expected. The orbits situated behind the shock, which occurs between sensors no. 15 and 16, have much greater amplitudes than those situated in front of the shock. This is due to the shock-induced, laminar–turbulent transition.

The method of analysis described here allows the detection of regions in a rather reliable way. However, it is not suited for making statements concerning the position of transition.

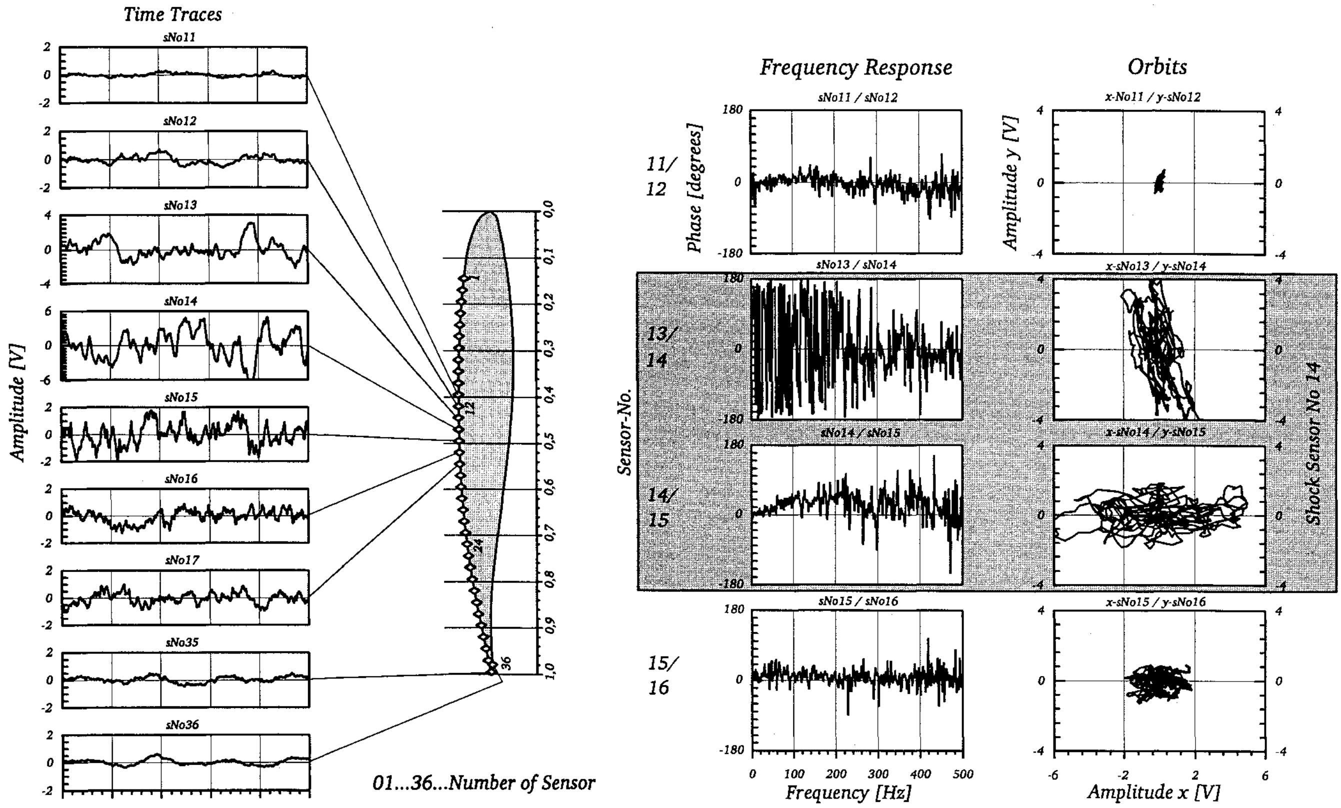

Fig. 9 Detection and proof of separation region by means of the phase shift and the orbits of two neighboring piezosensors for free transition, $M_\infty = 0.724$, $a = 3$ deg.

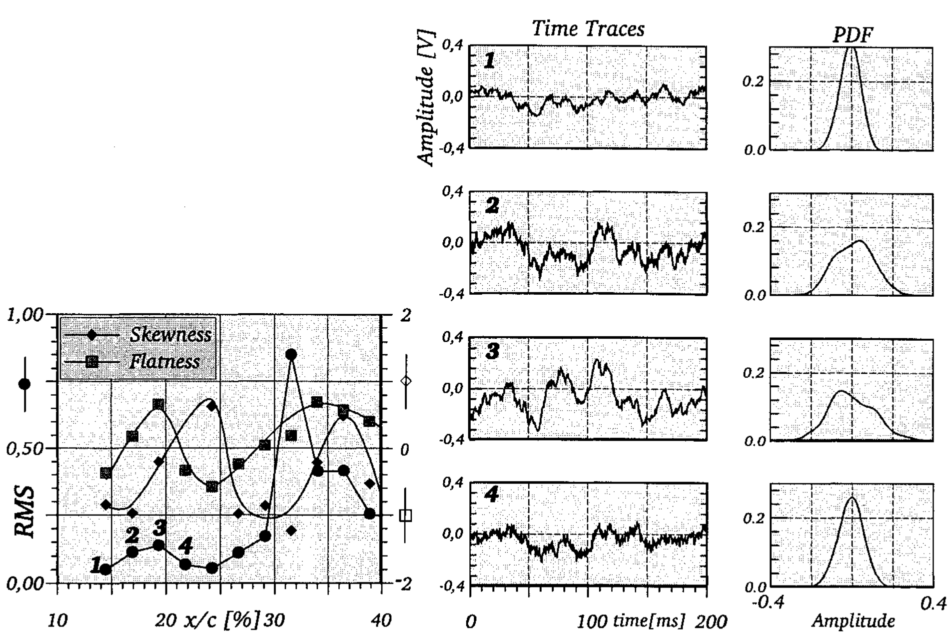

Fig. 10 Statistical evaluation of the piezofoil array signals in the region of transition for $M_\infty = 0.707$, $a = 3$ deg, and free transition.

The time signals and power spectra alone are likewise unsuited. For this reason, the time signals were evaluated statistically. As an example, Fig. 10 shows the distribution of the standard deviation (rms) as well as the skewness and flatness for a shock position of x/c = 32% in free transition. In addition, the time signals and the distribution of the probability density function (PDF) are shown for some sensors in this figure. By means of the high rms values, the shock occurring in the standard deviation is easily recognized. Apart from this, few conclusions about the position of transition can be drawn from the standard deviation. However, both skewness and flatness change their sign between sensors no. 2 and 3. When examining the distribution of the probability density, a sign change of the maxima is likewise recognizable. This is a reliable proof of transition because the transitional boundary layer intermittingly takes over the features of the laminar and turbulent boundary layer in this region. For this reason, the middle of the transition has to be exactly in the middle of the two sensors. Here, transition and the beginning of the separation bubble coincide (cf. Fig. 6).

Piezofoil Receiver

During the measurements carried out with a piezoreceiver, the pressure taps on the upper side of the airfoil were linked up to the sensors one after the other and the time signals mean-averaged 20 times. A result typical of such a measurement is shown for free transition in Fig. 11. Here, the shock occurs at pressure tap no. 14, x/c = 42% and is characterized by rather great amplitudes in the time signals. The separation bubble starts as early as position x/c = 25% (tap no. 18) and covers approximately 17% of the airfoil chord. In the power spectra of the autocorrelations in front of the shock a significant increase in power is to be recognizable between pressure taps no. 18 and 19. It is rather likely that the beginning of the separation bubble coincides with the beginning of the region of transition. Behind the shock, a distinct decrease in the density of power is to be seen. This applies, above all, to the lower frequencies. Both the autocorrelations and the power spectra show an almost constant course along the whole frequency region under consideration.

According to the observations presented previously, the transition position to be expected is thus found between 20–30% of airfoil chord in this flow configuration. To determine this position in a more exact way, it is likely to choose a case where the shock and, consequently, the beginning of the separation bubble are situated further at the back of the airfoil at a freestream Mach number of M_∞ = 0.749. The PDF was evaluated for pressure taps no. 15–20. Here, the shock lies at x/c = 62% and the beginning of the separation bubble at x/c = 36%. The results are shown in Fig. 12. Deliberately, the presentation was not standardized in order to illustrate possible differences between the laminar and turbulent flow. In the region of laminar flow (pressure tap no. 20), an almost Gaussian distribution of the probability density is recognizable. Further downstream, the maximum decreases and shifts towards positive amplitudes. A change of sign takes place between pressure taps 17 and 18. Thus, the region of transition is to be found within the region of these pressure taps. As a comparison, the distribution of the probability density in the turbulent region of the airfoil flow behind the shock (pressure tap no. 3) is also presented in this figure. Here, an almost Gaussian curve is likewise recognizable, although the course is flatter than in the laminar region.

For comparison, the deviation from the Gaussian standard distribution (skewness and flatness) was calculated for free and fixed transition. In Fig. 13 the courses of skewness and flatness are shown as well as the standard deviation (rms) and the two shock positions. In each case, an increase in the standard deviation up to the shock is clearly recognizable. At a shock position of 42% (free transition), a significant change of sign is to be found in the skewness and flatness at a x/c = 20–25%. Here, the beginning of the separation bubble and

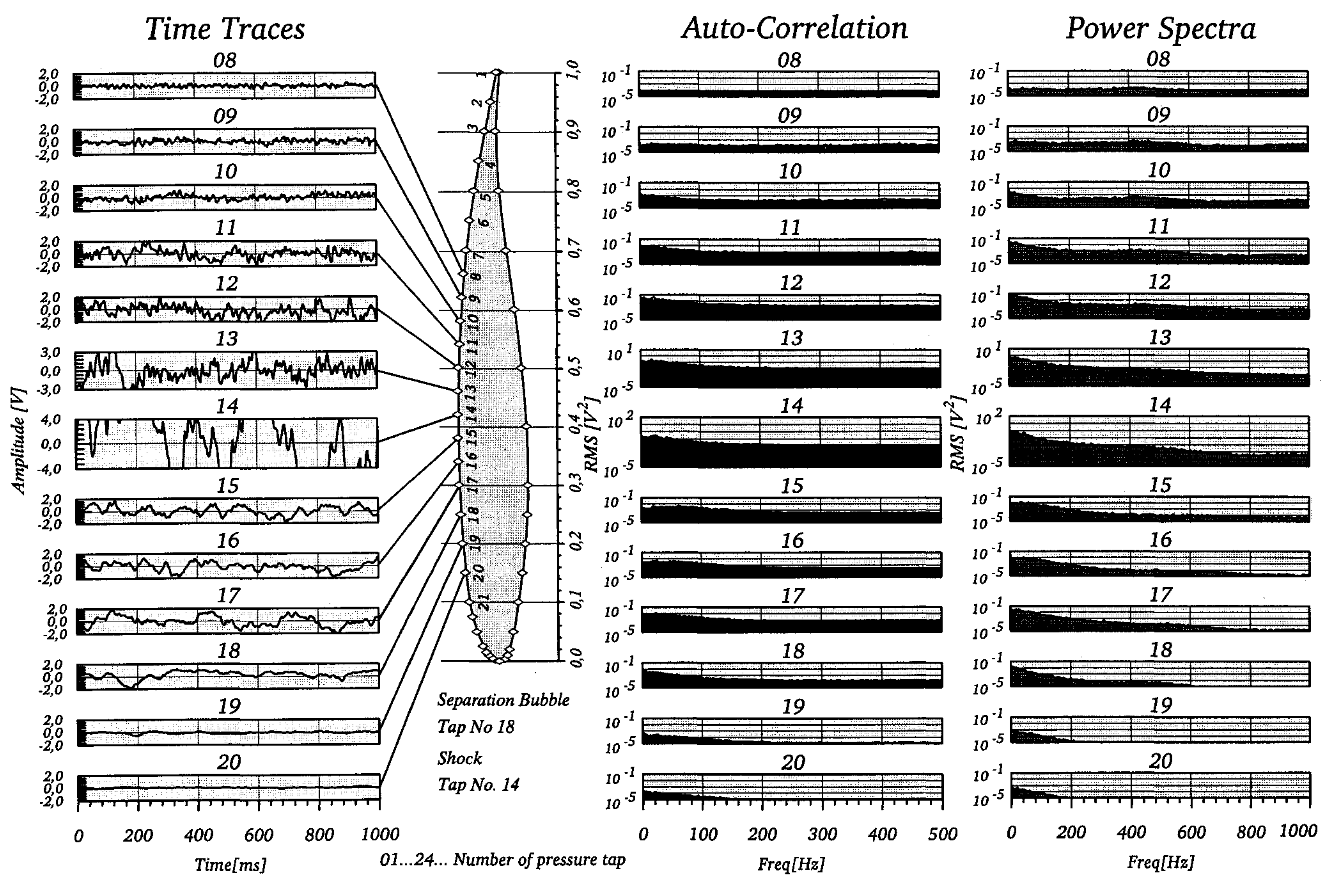

Fig. 11 Signals of the piezoreceiver for M_∞ = 0.744, a = 1 deg, free transition, autocorrelations, and power spectra.

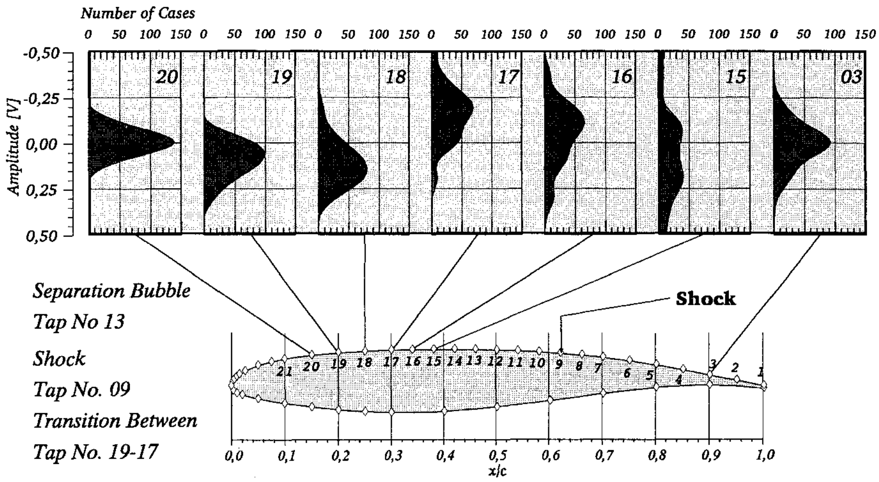

Fig. 12 Probability density functions for some pressure taps at M_∞ = 0.749, a = 1 deg, and free transition.

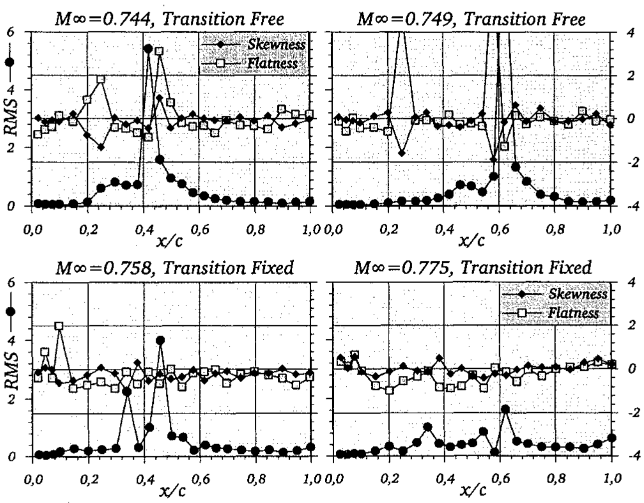

Fig. 13 Statistical evaluation of the signals of the piezoreceiver at a = 1 deg, rms, skewness, and flatness.

transition region coincide (see Fig. 13). Thus, the conclusion that the separation bubble practically compels transition can be drawn. In the case of the fixed transition, the beginning of the separation bubble in the rms values is rather distinct; both skewness and flatness change their signs behind the transition strip.

The states of the flow are to be defined most exactly at a shock position of 66%. Here, too, the beginning of the separation bubble at a position of x/c = 46% and the shock at x/c = 62% is to be seen from the strong increase in the standard deviation. Likewise, the transition region is to be identified in a rather good way by means of the skewness and flatness at the position of x/c = 25% (pressure tap no. 18). Thus, the observations presented earlier (see Fig. 12) were confirmed.

Concluding Remarks

With regard to the complex problem of the interaction between the shocks and boundary layer, numerous investigations concerning the interference between an originally laminar and a transition-fixed boundary layer on an airfoil, respectively, and shocks in a transonic flow around the airfoil model were carried out and compared in this article. Apart from conventional steady measurements (pressure and velocity) and flow visualization, unsteady surface measuring techniques were, above all, employed.

As early as in the steady pressure measurements did decisive differences between the laminar and transition-fixed flow show up. At the same freestream Mach number, the position of the shock on the airfoil is always located further downstream in the case of free transition. The local Mach number in front of the shock is, however, always smaller in this case. Thus, the flow starts to separate earlier behind the shock in a laminar boundary layer than in one where the transition is fixed. However, the pressure measurements show as well that the shock is always slightly curved in the upstream direction in the case of free transition. Thus, the flow is stabilized above the shock, because the streamlines are deflected behind the shock in the direction of the airfoil. This result was confirmed by global Laser-2-Focus measurements. For this reason, the flow accelerates once again behind the shock up to the supersonic region (a local postexpansion caused by the curvature of the airfoil), and continues to develop, up to a certain shock position, a multiple-shock configuration. These global phenomena have to do with the development of local regions of separation, which, on their part and with regard to their expansion and structure, strongly depend on the kind of boundary layer arriving. Thus, the flow visualizations carried out with oil showed that the separation bubbles in an originally laminar boundary layer, at least for the Reynolds numbers of $Re = 1.4 \times 10^6$ considered here, start considerably in front of the shocks and that they may extend up to 20% of the airfoil chord. In a transition-fixed boundary layer, these regions of separation are found below or behind the shock foot. Moreover, they are much smaller locally. For this reason, their effect on the airfoil flow is limited locally and, consequently, they are much smaller.

Two unsteady surface measuring techniques were used for analyzing in detail the region of interference. The first method was a piezoarray with 36 separate sensors that were mounted one after the other. By means of special techniques of analysis, which could be employed when simultaneously registering the time traces of several sensors, the regions of separation could also be detected in this case. Moreover, it became clear that the amplitudes of the time signals, and thus, the performance in the regular shock signals, are by far greater in the case of an originally laminar flow than in the case of fixed transition. This also applies when the point of transition, detected by means of the statical functions, was detected considerably far away upstream of the shock or from the beginning of the separation bubble. Thus, two different degrees of turbulence can be determined. Evidently, the degree of turbulence in the boundary layer caused by the transition strip was much greater here than in the case of free transition. The shock signal was more strongly absorbed due to the higher degree of turbulence. This seems to be the reason why an originally laminar boundary layer separates earlier behind the shock, although both the local Mach numbers in front of the shock and the pressure rise are smaller in this case.

In combination with the existing pressure taps of the airfoil, new types of receivers based on the piezofoil have been employed for measuring unsteady pressures in the shock boundary-layer interference region. By means of this new receiver, which was situated outside of the test section and linked to the pressure taps by means of pressure tubes, both the regions of separation and transition could be detected in an originally laminar flow. In conclusion, it can be stated that the piezoreceiver is a comparatively simple measuring technique, i.e., for investigating shock boundary-layer interferences (and here for detecting separation regions in particular) as well as determining transition.

Future research work investigating these problems will be concentrating on the detection of the phenomena characterizing the shock boundary-layer interference on a laminar airfoil configuration.

References

[1]Pearcey, H. H., Osborne, J., and Haines, A. B., "The Interaction Between Local Effects at the Shock and Rear Separation—A Source of Significant Scale Effects in Wind-Tunnel Tests on Aerofoils and Wings," CP-35, AGARD, 1968, pp. 11.1–11.23.

[2]Stanewsky, E., "Shock Boundary Layer Interaction," AGARD-AR-224, April 1988, pp. 271–305.

[3]Reshotko, E., "Shock Wave Boundary Layer Interactions," AGARD-AG-280, Feb. 1986.

[4]Pearcey, H. H., "A Method for the Prediction of the Onset of Buffeting and Other Separation Effects from Wind Tunnel Tests on Rigid Models," AGARD Rept. 223, 1958.

[5]Ganzer, U., Igeta, Y., and Ziemann, J., "Design and Operation of TU-Berlin Wind Tunnel with Adaptable Walls," International Council of Aeronautical Sciences Paper 64-2.11, 1984.

[6]Nitsche, W., Mirow, P., and Szodruch, J., "Piezo-Electric Foils as a Means of Sensing Unsteady Surface Forces," *Experiments in Fluids*, No. 7, 1989, pp. 111–118.

[7]Carraway, D. L., "Use of Piezoelectric Foils in Experimental Aerodynamics," *International Congress on Instrumentation in Aerospace Simulation Facilities '89 Record*, 1989, pp. 613–626.

[8]Nitsche, W., Swoboda, M., and Mirow, P., "Shock Detection by Means of Piezofoils," *ZFW*, Vol. 15, 1991, pp. 223–226.

[9]Bergmann, J. G., et al., "Pyroelectricity and Optical Harmonic Generation in Polyvinylidene Fluoride Films," *Applied Physics Letters*, Vol. 18, 1971, pp. 203–205.

[10]Swoboda, M., "Zum Einfluß der Stoß-Grenzschicht-Interferenz auf transsonische Profilströmungen," Ph.D. Dissertation, TU-Berlin, VDI-Verlag, Reihe 7, Nr. 230, 1993.

[11]Stack, J. P., Mangalam, S. M., and Kalburgi, V., "Phase Reversal Phenomenon at Flow Separation and Reattachment," AIAA Paper 88-0408, 1988.

[12]Scott, M. A., Carraway, D. L., and Lee, C. C., "A Comparison of Techniques for the Determination of Stagnation Location," *International Congress on Instrumentation in Aerospace Simulation Facilities '91 Record*, 1991.